Biochimica et Biophysica Acta 1798 (2010) 851–860

Contents lists available at ScienceDirect

Biochimica et Biophysica Acta

journal homepage: www.elsevier.com/locate/bbamem

A comparative study on the interactions of SMAP-29 with lipid monolayers

Frances Neville [a,b], Andrey Ivankin [c], Oleg Konovalov [d], David Gidalevitz [c,*]

[a] School of Process, Environmental and Materials Engineering, University of Leeds, Leeds, LS2 9JT, UK
[b] Centre for Multiphase Processes, School of Engineering, University of Newcastle, Callaghan 2308, NSW, Australia
[c] Center for Molecular Study of Condensed Soft Matter, Division of Physics, and Department of Biological, Chemical, and Physical Sciences, Illinois Institute of Technology, Chicago, IL 60616, USA
[d] European Synchrotron Radiation Facility, 6 Rue Jules Horowitz, BP 220, F-38043 Grenoble Cedex, France

ARTICLE INFO

Article history:
Received 15 May 2009
Received in revised form 8 September 2009
Accepted 24 September 2009
Available online 2 October 2009

Keywords:
Peptide–lipid interactions
Antimicrobial peptide
Langmuir monolayer
X-ray scattering

ABSTRACT

This work investigates the discrimination of lipid monolayers by the ovine antimicrobial peptide SMAP-29 and compares it to that of the human LL-37 peptide. Fluid phospholipid monolayers were formed in a Langmuir trough and subsequently studied with the X-ray scattering techniques of X-ray reflectivity and grazing incidence X-ray diffraction. Any changes in the phospholipid structure after injection of peptide under the monolayer were considered to be due to interactions between the peptides and lipids. The data show that SMAP-29 discriminates against negatively charged phospholipids in a similar way to LL-37. However, it is even more interesting to note that despite a higher concentration of SMAP-29 near the monolayer, ensured by its greater charge as compared to LL-37, the amount of SMAP-29 needed to observe monolayer disruption was around three and a half times the number of molecules of LL-37 used to see similar changes with the same system. This result suggests that the structure, amino acid sequence or size of the peptide may well be as important as electrical charge and therefore gives many implications for the further study of antimicrobial peptides with regards to novel drug design and development.

1. Introduction

The last decade has seen a considerable increase in the study of antimicrobial peptides and their mimics due to the interest for their potential as future pharmaceutical drug compounds [1–3]. Although it is evident that the cell membrane is a barrier which must be overcome by antimicrobial peptides for cell disruption, the mechanisms of action of all antimicrobial peptides remain unclear [4]. It has been proposed that antimicrobial peptides exhibit cell selectivity by being more toxic to micro-organisms than to host cells [4–7]. One of the main reasons for this is thought to be due to the different lipid components and physical properties of the cell membranes involved.

SMAP-29 is an α-helical peptide of ovine origin [8–9] and the sequence has been determined as: RGLRRLGRKIAHGVKKYGPTVL-RIIRIAG [9]. The peptide has a net charge of +10 and a molecular mass of 3257. The charges in the SMAP-29 molecule originate from six arginine (R) residues, three lysine residues (K) and one histidine (H) residue. The molecule only contains positively charged residues to gain its charged properties, unlike the only human cathelicidin peptide, LL-37 (LLGDFFRKSKEKIGKEFKRIVQRIKDFLRNLVPRTES) which contains both positively and negatively charged residues [7,10–12].

Tack et al. [9] confirmed the work of Bagella et al. [13] regarding the structure of SMAP-29. They used nuclear magnetic resonance and circular dichroism to show that SMAP-29 contains an α-helical section followed by an extended region joined by a hinge at residues 18–19 (glycine and proline). Tack et al. [9] also showed that there was an ordered hydrophobic section between residues 20 and 28, and that SMAP-29 was flexible in 40% trifluoroethanol and formed two sets of conformers that were different with regards to their orientation relative to the N-terminal domain [9].

SMAP-29 is active against many potent bacterial strains including *Escherichia coli, Salmonella typhimurium, Pseudomonas aeruginosa, Saccharomyces aureus* and *Enterococcus faecalis* [8,11,14–16] but unlike LL-37, it also has antifungal properties [8,17].

The understanding of the mechanism of interaction between SMAP-29 and cell membranes of different types has not been fully developed. However, there is some work investigating the effect of SMAP-29 on cell and lipid systems with regards to cell selectivity and its mechanism of action [8,17–19].

The mechanism of action of SMAP-29 was investigated by Lee et al. [17]. They found that SMAP-29 accumulates in the plasma membrane. Lee et al. [17] also carried out experiments with lipo-somes composed of phosphatidylcholine (PC) lipids and mixtures of PC and cholesterol to observe the disruptive effect of SMAP-29 on cell

Abbreviations: SMAP-29, sheep myeloid antimicrobial peptide-29; GIXD, grazing incidence X-ray diffraction; XR, X-ray reflectivity; ESRF, European Synchrotron Research Facility; DPPG, dipalmitoylphosphatidylglycerol; DPPC, dipalmitoylphosphatidylcholine

* Corresponding author. Tel.: +1 3125673534; fax: +1 3125678874.
E-mail address: gidalevitz@iit.edu (D. Gidalevitz).

0005-2736/$ – see front matter © 2009 Elsevier B.V. All rights reserved.
doi:10.1016/j.bbamem.2009.09.017

membranes. The authors suggest that membrane disruption by SMAP-29 occurs via pore formation, although the complete mechanism of action is still unclear.

McGwire et al. [18] investigated the mechanisms of action of SMAP-29 and its analogues as possible treatments for the protozoan parasitic infection caused by *Trypanosoma brucei*. They found that the peptides were effective in killing the parasite in both the insect and bloodstream forms. According to these authors [18], the mechanism of action against the parasite involves disruption of surface membrane integrity as is the case with other microbes, such as *E. coli* and *S. aureus* which were studied by Anderson et al. [19]. However, the precise mechanism of action remains to be elucidated. As well as this, previous studies on SMAP-29 have not addressed how SMAP-29 can discriminate between different lipid types and this has been studied with other peptides and is a major attribute of antimicrobial peptides.

The interactions of phospholipid monolayers with SMAP-29 have not been investigated previously. However, the same lipid monolayer systems have been used to study the interactions of the porcine antimicrobial peptide protegrin-1 [6] and the human antimicrobial peptide LL-37 [7] using X-ray scattering techniques. Previously published results [7] indicate that there is very little interaction between LL-37 and the di-palmitoylphosphatidylcholine (DPPC) monolayer at the concentrations that were used (8.9 nM and 22.3 nM). This is in contrast to results for the dipalmitoylphosphatidylglycerol (DPPG) monolayer system [7] whose structure was completely destroyed after injection of LL-37 even at the low concentration of 8.9 nM. The work by Neville et al. [7] also supports previous research [20–23] suggesting that the human antimicrobial peptide LL-37 acts against bacterial membranes via the “carpet” mechanism of membrane perturbation with consequent micellation.

The carpet mechanism of membrane perturbation [22] consists of a process which involves the covering of the membrane surface with peptides, progressing to direct membrane disruption or the formation of toroidal pores followed by the possible formation of peptide-induced peptide–lipid micelles. However, little evidence exists of the formation of micelles induced by cathelicidin antimicrobial peptides such as LL-37. It has been proposed that this evidence was presented previously by Neville et al. [7], whilst studying the effect of LL-37 on DPPG monolayers in a fluid system by using epifluorescence microscopy ([7], Fig. B6). More recently, in agreement with the previous work on LL-37 interactions [7], Sevcsik et al. [23–24] have proposed that LL-37 causes membrane disruption in different ways not only depending on the type of lipid head group, but also on the hydrocarbon chain length. Also in agreement with our findings [7], Sevcsik et al. [23] show that the model DPPG layer is decreased in thickness on perturbation by LL-37. However, they propose the formation of peptide-induced micelles with the DPPC lipid rather than DPPG. It has been previously suggested that variation in results may be explained by different experimental approaches [23] and therefore future work on LL-37 interactions which combines the methodologies and model systems used might be able to provide a more detailed insight into the mechanism of action of LL-37.

The proposed molecular basis for membrane discrimination by antimicrobial peptides [25] suggests that hydrophobic interactions are in place in all peptide-membrane interactions but that cationic peptides are more strongly attracted to prokaryotic membranes due to the electrostatic forces present between the positive charged peptides and the negatively charged bacterial membranes [25]. In this case the initial binding, or attraction of the peptides to membranes, is due to electrostatic interactions which play a crucial role in ensuring an increased concentration of peptide near the membrane surface [26–27]. Electrostatic forces may also be important during adsorption at the membrane surface or during insertion. However, the individual contribution of electrostatic forces during adsorption or insertion is difficult to ascertain and it has been proposed that other factors such as peptide size, structure, hydrophobicity and charge distribution may influence the interaction of antimicrobial peptides with different types of membranes. Sevcsik et al. [24] have proposed that lipid net charge is not the main factor which determines the mechanism of action of LL-37 interactions with model membrane systems.

This paper shows that two very similar systems behave differently when the peptide used is the main variable. Our results show that the SMAP-29 peptide (which has a lower molecular mass and is more cationic) interacts with negatively charged lipid monolayers to a lesser extent than the LL-37 peptide, which has a greater molecular mass and is less cationic, even when a 38% molar excess of SMAP-29 was used. Therefore, peptide amino acid sequence, size and conformation are likely to be as important as its charge distribution.

2. Materials and methods

2.1. Materials

DPPC and DPPG lipids were purchased from Avanti Polar Lipids (Alabaster, USA) and were used without further purification. All experiments were performed using Dulbecco's phosphate buffered saline (DPBS) (Invitrogen, Carlsbad, USA) without calcium and magnesium ions. Monolayers of DPPC were deposited from chloroform solution (high performance liquid chromatography grade, Fisher Scientific, Pittsburgh, USA), whereas DPPG was deposited from a 9:1 v/v% chloroform/methanol solution (high-performance liquid chromatography grade, Fisher Scientific). LL-37 and SMAP-29 (90–95% pure) were supplied by Pepceuticals (Nottingham, UK). LL-37 and SMAP-29 peptides were provided as solid powders and made up to stock solutions (0.1 mg/ml peptide in 0.01% glacial acetic acid w/v) before being further diluted for the working solutions (10 μg/ml peptide in 0.01% glacial acetic acid w/v). Acetic acid (Fisher Scientific) was used to maintain the peptide structure while in solution.

2.2. Lipid monolayers

To investigate peptide-membrane interactions, Langmuir monolayers composed of lipids representative of membranes were studied. Monolayers can be used as mimics of the outer leaflets of cell membrane bilayers and this approach has been utilised repeatedly over the years [28–33]. The planar monolayer system allows versatile adjustments of parameters such as monolayer composition, surface pressure, packing density and aqueous subphase properties in order to model the conditions under which peptides interact with cell membranes. The cell membranes of different organisms have characteristic lipid compositions. However, to develop a full understanding of membrane interactions, individual components of membranes were studied separately to ascertain the contribution of each membrane component to the overall interaction of the peptide with the membrane. In this research DPPC and DPPG were used to form Langmuir monolayers at the air–aqueous interface to mimic the outer leaflet of the erythrocyte cell membrane and the surface of the bacterial cell wall, respectively. The subphase temperature was maintained at 22 ± 1 °C for lateral compression and X-ray scattering experiments.

2.3. Pressure-area compression isotherms

Upon spreading, the lipid film was left undisturbed for 15 min to allow time for the solvent to evaporate. At this point, barrier compression (at 2 cm^2 min^{-1}) was initiated and the increase in surface pressure of the monolayer was monitored until the target pressure was attained. This compression gives rise to a surface pressure (mN/m) versus area per lipid molecule ($Å^2$/molecule) isotherm, which can be utilised to observe the phases and phase transitions associated with the monolayer as a function of area per lipid molecule.

2.4. Pretreatment experiments

Pretreatment experiments check the inserted peptide's ability to sustain its position in the monolayer at high lipid packing densities. In a typical pretreatment experiment, the lipid was deposited and the solvent was left to evaporate for 15 min. While holding the barriers at the fully expanded position, the peptide was injected uniformly into the subphase under the monolayer using a microsyringe with an "L-shaped" needle (VDRL needle; Hamilton, Reno, Nevada, USA) to make up the final concentration required in the subphase. Peptide concentrations of 0.04 μg/ml and 0.1 μg/ml were used. The molar ratio of SMAP-39 to LL-37 was 1.38 to 1. They are well below the minimum inhibitory concentration (MIC) for both peptides used. In the case of SMAP-29 the above concentrations correspond to 12.3 nM and 30.7 nM, respectively, and the MIC is 120–767 nM for various different types of bacteria [8,20]. For LL-37 the MIC is 0.2–28 μM and the concentrations used were 8.9 nM (0.04 μg/ml) and 22.3 nM (0.1 μg/ml). Any change in surface pressure as a result of peptide incorporation into the lipid monolayer was monitored. The monolayer was left to equilibrate for 15 min after peptide injection. The lipid/peptide film was then compressed by closing the barriers while its pressure-area isotherm was recorded. These types of experiments have been termed "pretreatment" since the lipid layer is "pretreated" with the peptide before compression and the other lipid with peptide experiments carried out using the Langmuir trough (insertion experiments) involve compression of the lipid before peptide injection. The pretreatment experimental method has been successfully used with lipid A monolayers [34] and polymers [35–36], but has not been previously used to examine the types of lipid-peptide system presented here.

2.5. Insertion experiments

Insertion experiments were carried out to quantify the interaction of the peptide with the lipid monolayer. Initially, the lipid monolayer was deposited and equilibrated, followed by compression to the surface pressure corresponding to the liquid-condensed phase of lipids (30 mN/m), and equivalent to the packing density of real cell membranes [37–38]. The surface pressure was kept constant via a built-in proportional-integral-derivative control feedback system by adjusting the surface area. The peptide solution (10 μg/ml peptide in 0.01% glacial acetic acid w/v) was then evenly injected underneath the monolayer in the same way as for the pretreatment experiments to make up the required final bulk concentration. Once the peptide is injected, its interaction with the lipid monolayer results in an increase in the surface area since the surface pressure is being kept constant. The resulting relative change in area per molecule, $\Delta A/A$, was monitored throughout the experiment to compare the degree of peptide insertion into the DPPC and DPPG monolayers.

2.6. Peptides at the air–liquid interface

The peptides are soluble in water, but, being amphipathic [9,39] are expected to be adsorbed at the air–liquid interface. SMAP-29 was injected into the pure subphase without a lipid monolayer present. The properties of the pure SMAP-29 monolayer were then investigated using pressure-area isotherms in conjunction with X-ray reflectivity (XR) and grazing incidence X-ray diffraction (GIXD) and compared to those of the LL-37 film [7].

2.7. Langmuir troughs

Pressure-area compression and pretreatment isotherms were performed using a twin-barrier rectangular Teflon micro Langmuir–Blodgett trough equipped with a Wilhelmy plate (Nima Technology, Coventry, UK). Insertion experiment data were obtained using a custom-built trough [40–41] at the University of Chicago. X-ray scattering measurements were taken at the European Synchrotron Radiation Facility (ESRF) utilising a custom-built Langmuir trough equipped with a single moveable barrier [28,42].

2.8. GIXD and XR

Surface X-ray scattering experiments were carried out at the ID10B (Troïka II) beam line at the ESRF (Grenoble, France). The trough was completely sealed by a cover before experiments were carried out. The oxygen level was subsequently monitored as the air inside the covered trough system was replaced with water-saturated helium in order to reduce evaporation and scattering from the air. The oxygen level was allowed to reach a sufficiently low level before measurements were commenced (<0.1%). Control measurements of pure lipid monolayers were followed by subsequent injection of the desired amount of peptide into the subphase under the monolayer-covered area of the surface at 30 mN/m.

Grazing incidence X-ray diffraction (GIXD) [43] was used to obtain in-plane information concerning the molecular structure of surfaces [44]. GIXD measurements were made with variation of the X-ray momentum transfer component q_{xy} that is parallel to the air–aqueous interface. Such a configuration enables the incident wave to be reflected, whereas the refractive wave propagates along the surface, making this technique very sensitive to changes at the air–aqueous interface. The reflections of the Bragg peaks observed with this geometry can be indexed by two Miller indices, *hk*. Their angular position $2\theta_{hk}$, corresponding to $q_{hk} = (4\pi/\lambda) \sin \theta_{hk}$, yields the repeat distance $d_{hk} = 2\pi/q_{hk}$ for the two-dimensional (2D) lattice structure. Bragg peak profiles (intensity against q_{xy}) were fitted with Gaussians and the peak position values were used to obtain unit-cell dimensions of the lipid lattices. The observation of two Bragg peaks in the diffraction pattern of an amphiphilic monolayer is indicative of a distorted hexagonal unit cell (which may be better described as a centered rectangular unit cell) [6]. Therefore, all unit-cell dimensions in this paper have been calculated using the centered rectangular unit cell approximation.

Specular X-ray reflectivity (XR) measurements reveal information on the electron-density distribution along the surface normal and may be used to determine the density and thickness of thin films [31,43,45]. When specular X-ray reflectivity occurs, the scattering vector q_z may be calculated from $q_z = 4\pi/\lambda \sin \alpha$, where α is the grazing angle of the incident beam and λ the wavelength of the X-ray beam. The reflectivity curve of intensity against q_z contains information regarding the gradient of the electron-density profile in the direction normal to the surface [46–47]. XR measurements were carried out over a range of angles corresponding to q_z values of 0–0.65 $Å^{-1}$. The reflected beam intensity was measured as a function of the incident angle using a position sensitive detector.

The XR data were then analysed using data processing and fitting programs as carried out previously [7,28,34], in order to gain information on the electron density distribution in the direction normal to the surface. This provided an electron density profile averaged laterally over both ordered and disordered parts of the system. The whole monolayer and subphase system was modelled as slabs, or layers, where each slab has a constant electron density and thickness [28].

3. Results and discussion

3.1. SMAP-29 film structure at the air–aqueous interface

Although the structure of SMAP-29 has been shown to be unstructured in aqueous solutions [9], a peptide monolayer film formed at the air–aqueous interface when peptide was injected

into the subphase in the Langmuir trough. This has been shown by investigating the properties of SMAP-29 using X ray reflectivity.

X-ray reflectivity data for SMAP-29 (Fig. 1) were analysed [28,46] after injection of SMAP-29 inside the buffer using a constant area of the trough. After injection, the surface pressure increased slightly to 1 mN/m. The best fit of the reflectivity data at 1 mN/m was obtained using a two slab model. The fitting of the data returned values of 12.6 Å and 11.1 Å for the two slabs going from the air–aqueous interface towards the subphase, respectively. Corresponding electron density values normalised to the electron density of the subphase ($0.337\ e^{-}\ Å^{-3}$) for the slabs were obtained as 1.31 and 1.04. Due to the known [9] dimensions of the SMAP-29 molecule (approximately 26 Å×12 Å×16 Å), the data suggest that there is single SMAP-29 layer formed at the air–aqueous interface with the more hydrophilic residues oriented towards the subphase.

The SMAP-29 XR data (Fig. 1) show similarities to LL-37 XR data [7] as the shape of the curve of data is alike and there are no defined structural features such as can be seen for DPPC and DPPG lipids [7]. This suggests that the SMAP-29 peptide layer is disordered, as mentioned earlier [9] and such as is seen with other protein structures at the air–aqueous interface [25,48].

3.2. Interaction of cathelicidin peptides with DPPC monolayers

Although the design of novel antimicrobial drugs involves thorough testing on a variety of micro-organisms, it is also necessary to test the cytotoxicity of the drug on the host cells. Since PC lipids are the most abundant lipid type contained in the outer leaflet of human red blood cell membranes [49], DPPC lipids were used to observe the interactions of the antimicrobial peptides with lipid monolayers composed of these lipids.

3.2.1. Pretreatment experiments

The pretreatment method was carried out in order to determine whether the peptide could be forced out from its position at the air–aqueous interface, by the competing lipids, when the pressure was increased. The pretreatment experiments of LL-37 and SMAP-29 systems presented here for the first time are compared and contrasted.

Fig. 2 shows pretreatment data for the DPPC with LL-37 and SMAP-29 systems. Fig. 2 shows the isotherms of the pretreatment experiments using two different concentrations of LL-37 (8.9 and 22.3 nM) and 12.3 nM SMAP-29. It also contains the π-A isotherm for the pure DPPC lipid and pure LL-37 film for comparison. The pure LL-37 film has been previously discussed and it is thought that under compression the peptide aligns at the air–aqueous interface in a similar manner to the PGLa peptide [7]. All measurements were carried out on the same trough (Nima Technology). The LL-37 isotherm is presented with the area per molecule scale reduced to one quarter of its actual value, for better comparison of data. Fig. 2 shows that injection of 8.9 nM LL-37 gave a pressure increase of 1–2 mN/m and injection of 22.3 nM LL-37 gave a pressure increase of around 8–10 mN/m.

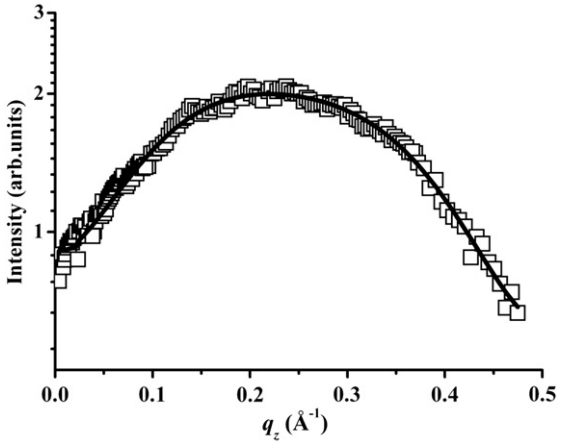

Fig. 1. Reflectivity data (squares) and corresponding fit (line) of the SMAP-29 layer.

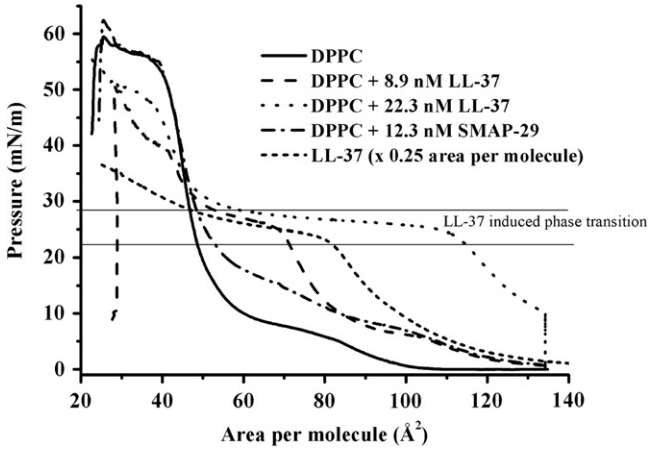

Fig. 2. Pressure-area isotherm of DPPC with and without pretreatment with LL-37 and SMAP-29. The LL-37 isotherm is also presented as one quarter scale on the area per molecule axis. Liquid-expanded, Liquid-expanded–liquid-condensed and liquid condensed phases are represented as LE, LE-LC and LC, respectively.

The pretreatment isotherm (Fig. 2) of DPPC with LL-37 (8.9 nM), shows that there is an increase in pressure at area per DPPC molecule values of approximately 50 to 140 Å^2/molecule, in comparison to the pure DPPC isotherm. It is clear that this increase in pressure is mainly due to the LL-37 present at the air–aqueous interface. Nevertheless, the plateau region of the lipid phase transition of DPPC from the liquid-expanded to the liquid-expanded liquid-condensed co-existence region can still be seen at around 8 mN/m. However, the presence of LL-37 at the interface has shifted the phase transition to the right by around 20 Å^2/molecule from the value seen in the pure DPPC isotherm, showing that the LL-37 is interacting with the DPPC in some way. An extra phase transition can be seen in the data at around 25–28 mN/m and may be due to the presence of LL-37 at the air–aqueous interface (Fig. 2).

When using the higher concentration of LL-37 (22.3 nM), there was a substantial increase in pressure when the LL-37 was injected under the lipid monolayer before compression. This is shown by the vertical section of the curve (dotted line, Fig. 2). Therefore, because of this initial pressure increase, the liquid-expanded and liquid-expanded liquid-condensed phases observed with the lower concentration of LL-37 (8.9 nM) are no longer present, and the isotherm proceeds to the same phase transition seen with the LL-37 isotherm at around 25–28 mN/m. The LL-37 isotherm is discussed further in Neville et al. [7].

The LL-37 peptide does not remain in DPPC films at high pressure as the pretreatment isotherm returns to values close to those of the pure DPPC isotherm. This suggests that at higher pressures (~ 30 mN/m) and lower areas (~ 45 Å^2 per molecule) the LL-37 is forced out from its position at the air–aqueous interface, leaving a film enriched in DPPC molecules.

The results of the DPPC with SMAP-29 pretreatment experiment are also shown in Fig. 2. The data show that the liquid-expanded lipid phase is present in both the pure DPPC isotherm and the DPPC with SMAP-29 pretreatment isotherm (Fig. 2). However, the DPPC with SMAP-29 pretreatment isotherm is shifted to the right by approximately 25 Å^2 per DPPC molecule units. This suggests that SMAP-29 is present at the air–aqueous interface. The results show that SMAP-29 goes to the surface at low pressures but is pushed away from the air–aqueous interface (out of the DPPC monolayer)

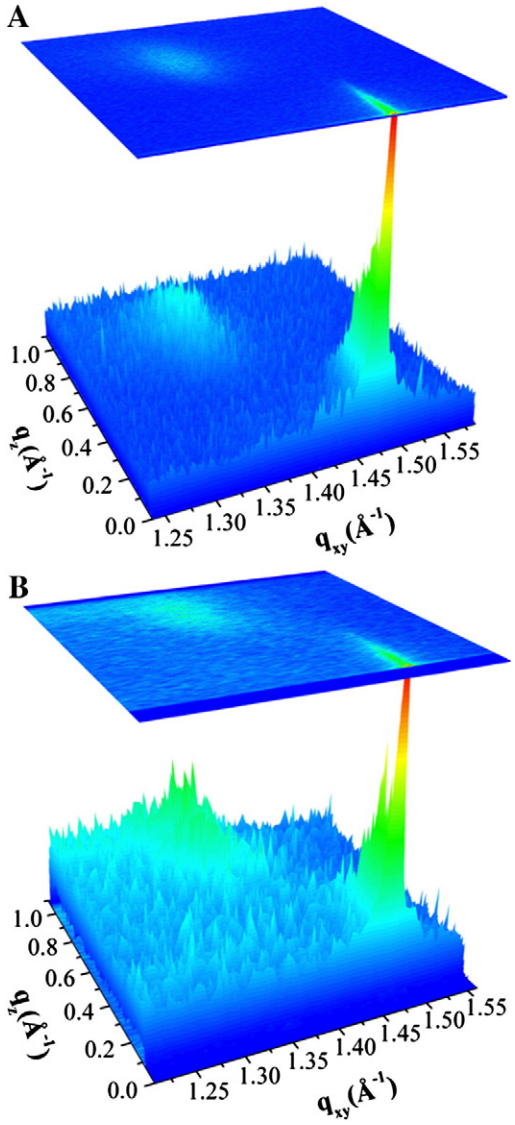

Fig. 3. 3D plots of Bragg peaks (q_{xy}) against Bragg rods (q_z) as a function of intensity. (A) DPPC 30 mN/m monolayer before injection. (B) after injection of 30.7 nM SMAP-29.

after compression to around 30 mN/m. This is seen from the fact that the isotherm reverts to the same values of pressure and area as the pure DPPC isotherm at pressures higher than 30 mN/m. Overall, the data indicate that SMAP-29 goes to the surface when there is space but it is not retained in the DPPC monolayer. This is similar to the DPPC with LL-37 system, although the pretreatment data clearly show the presence of LL-37 at the air–aqueous interface and not in the presence of SMAP-29.

3.2.2. Insertion isotherms

Insertion isotherms with DPPC and DPPG systems using the LL-37 peptide have been previously carried out [7]. Insertion isotherms using DPPC monolayers showed that in general there was a very small increase in area on injection of peptide into the subphase under constant pressure conditions (30 mN/m) [7]. Here we present work on the interactions of SMAP-29 with lipid monolayers where the difference compared to previous work with LL-37 is the type and molar concentration of peptide we have used. Therefore, it is interesting to compare the insertion patterns of LL-37 and SMAP-29.

Pretreatment experiments (Fig. 2) showed that the SMAP-29 was not retained in the DPPC monolayer when the subphase concentration before compression was 12.3 nM. Therefore, it was thought that it would be even less likely to insert into a preformed DPPC monolayer at 30 mN/m and so insertion isotherms were carried out with 30.7 nM SMAP-29.

It could be assumed that the insertion isotherm for DPPC with 30.7 nM SMAP-29 (Fig. 1S, supplementary data) should allow a greater possible change on peptide insertion than using 12.3 nM SMAP-29. However, even when using the higher concentration of SMAP-29, the system showed no insertion of SMAP-29 into the DPPC monolayer (Fig. 1S, supplementary data). The area per molecule value remained stable, varying only slightly from the start point (Fig. 1S, supplementary data). This suggests that the SMAP-29 peptide is not attracted to the DPPC covered surface when the pressure of the DPPC monolayer is 30 mN/m. This is consistent with the pretreatment experiments (Fig. 2) which show that SMAP-29 is forced out from the surface after pressures of higher than 30 mN/m are reached.

3.2.3. Grazing incidence X-ray diffraction

Grazing incidence X-ray diffraction measurements were taken at 30 mN/m when the lipid is in the liquid-condensed phase. In corroboration with the pretreatment experiments (Fig. 2) and insertion assays (Fig. 1S, supplementary data), little change in DPPC packing pattern was observed following SMAP-29 injection at 30 mN/m (Fig. 3B). After injection of 30.7 nM SMAP-29 under the DPPC monolayer (Fig. 3B), the peak positions yield *d*-spacings of 4.64 Å and 4.28 Å. This computes to unit cell dimensions of $a = 5.52$ Å, $b = 8.56$ Å and an area per molecule of 47.2 Å^2 showing little interaction of SMAP-29 with the phosphatidylcholine head groups, since the area per molecule from the pure DPPC monolayer is 46.6 Å^2. This is very similar to the results of the DPPC at 30 mN/m with 8.9 nM LL-37 system, which gave an area per molecule of 47.1 Å^2 [7]. Although the higher concentration of SMAP-29 (30.7 nM) is presented here, the results were the same as for the lower SMAP-29 peptide injection (12.3 nM), despite the two and half times increase in concentration. It should be noted that the GIXD DPPC control data presented (Fig. 3A) were previously published (Fig. 6, A1 [7]) when comparing the DPPC monolayer before and after injection of LL-37 peptide.

3.2.4. X-ray reflectivity

In addition to the previous results (Figs. 2–3), XR data for the DPPC monolayer after SMAP-29 injection show little variance from the data for the pure DPPC monolayer (Fig. 4), This is consistent with selectivity of antimicrobial peptides between host and bacterial membranes. The data of the DPPC with SMAP-29 system were modelled as a two-slab system, as was the DPPC with LL-37 system [7]. The fit to the data of the system where SMAP-29 (30.7 nM) was injected under

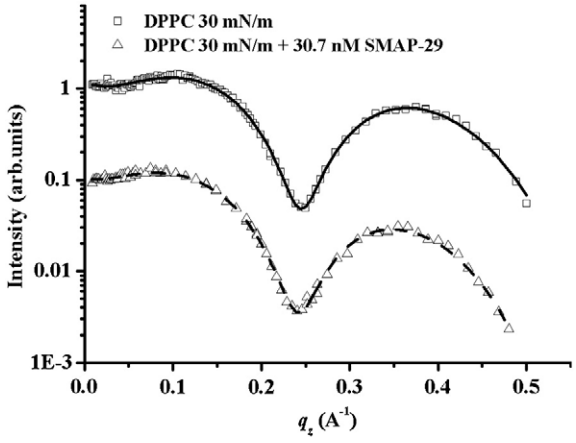

Fig. 4. X-ray specular reflectivity data (symbols) and corresponding fits (lines) normalised by Fresnel reflectivity plotted against scattering vector q_z. Data of DPPC monolayer at 30 mN/m before injection (squares) and after 30.7 nM SMAP-29 injection (triangles). For clarity the data have been offset vertically.

the DPPC monolayer gave values similar to those for the pure DPPC monolayer [7]. The tail slab was found to be 16.1 Å thick and the respective electron density for this layer normalised to the electron density of the subphase (0.337 e^{-} $Å^{-3}$) was 0.92, whereas the head slab was 7.6 Å thick with a normalised electron density of 1.33. These values are comparable to those obtained for a pure DPPC monolayer using XR [7] where the tail slab was 15.2 Å thick, with a normalised electron density of 0.91 and the headgroup was 8.8 Å thick with a normalised electron density of 1.33.

3.3. Interaction of cathelicidin peptides with DPPG monolayers

The results of the experiments using negatively charged DPPG monolayers representing the bacterial surface layer are presented below. DPPG lipids are substantial components of both Gram-positive cell membranes and the inner membrane of Gram-negative bacteria. The interactions of SMAP-29 and LL-37 with DPPG monolayers were observed using pretreatment experiments. Insertion assays, GIXD and XR were further used to characterise the interactions of SMAP-29 with DPPG monolayers, and to compare the results with the previously published DPPG monolayer with LL-37 results [7].

3.3.1. Pretreatment experiments

Fig. 5A shows the data of the pretreatment experiments carried out for DPPG with LL-37 systems, using two concentrations of LL-37 (8.9 and 22.3 nM). Fig. 5 also shows the isotherms of pure DPPG and LL-37

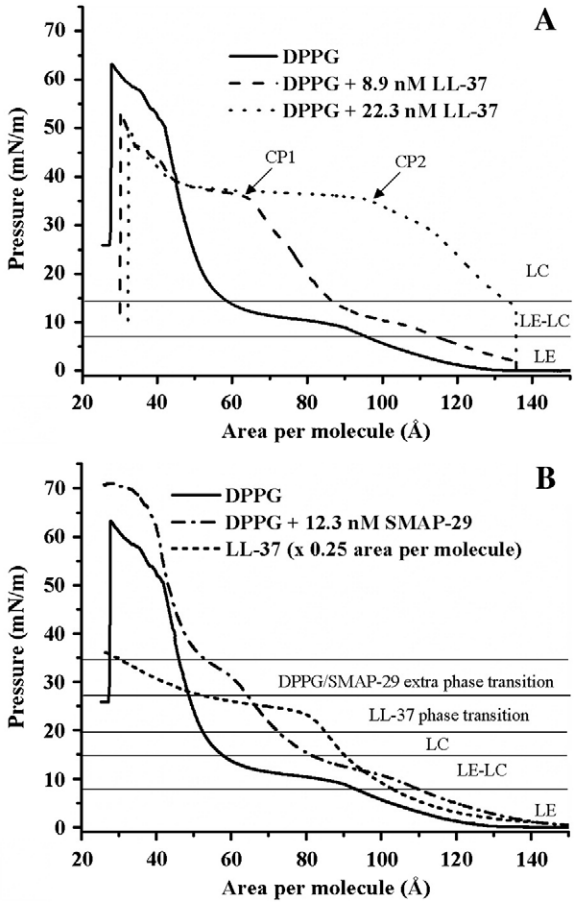

Fig. 5. Pressure-area isotherm of DPPG with and without pretreatment with (A) LL-37 and (B), SMAP-29. The LL-37 isotherm is also presented as one quarter scale on the area per molecule axis. Liquid-expanded, Liquid-expanded–liquid-condensed and liquid condensed phases are represented as LE, LE-LC and LC respectively. The beginning of collapse of the system DPPG with 8.9 and 22.3 nM LL-37 are represented with CP1 and CP2, respectively. The LL-37 phase transition and extra SMAP-29/DPPG phase transition are indicated in the figure.

for comparison. The lipid phase transition between the liquid-expanded and liquid-expanded-liquid-condensed coexistence phases is observed with the DPPG and 8.9 nM LL-37 system (9–13 mN/m), as was also the case for the DPPC with 8.9 nM LL-37 system at approximately 6–10 mN/m (Fig. 2). However, the beginning of collapse of the DPPG with 8.9 nM LL-37 system (CP1, Fig. 5A) can be seen at a much earlier stage than for the equivalent DPPC system seen in Fig. 2. In the figure CP, refers to the point at which collapse begins where the surface tension is disrupted and there was overspill visually observed even though complete collapse (a sudden drop in surface pressure) was not observed until around 30 $Å^2$/molecule.

When the pretreatment experiment for the DPPG with LL-37 (22.3 nM) system was carried out, the beginning of collapse (CP2, Fig. 5A) was visually observed at a value of around 100 $Å^2$ /molecule which is much higher than the value for the pure DPPG monolayer which begins to collapse at around 41 $Å^2$/molecule. The data suggest that the LL-37 binds strongly to the DPPG lipid (at both concentrations used), and that some kind of DPPG/LL-37 complex is formed at the air–aqueous interface. On compression there is not enough room for this combined DPPG/LL-37 system to remain at the surface and thus the surface film becomes unstable and collapses. This discrimination by LL-37 has been further corroborated by other experimental techniques previously carried out [7].

For comparison with the DPPC experiment (Fig. 2), the DPPG pretreatment experiment was also carried out with 12.3 nM SMAP-29. The results of the DPPG pretreatment experiment (Fig. 5B) are somewhat different to those of the DPPC experiment (Fig. 2). The DPPG with SMAP-29 is similar to that of the DPPC with SMAP-29 pretreatment isotherm at high values of area per molecule. However, there are two main differences after the pressure reaches approximately 15 mN/m. Firstly, the presence of an extra phase transition is seen in the DPPG with SMAP-29 isotherm at around 33 mN/m. This shows similarities to the pretreatment isotherm of the DPPC with LL-37 system (Fig. 2) where it was suggested that the extra phase transition was due to the presence of peptide at the air–aqueous interface, although in this case the extra phase transition is at a higher pressure value and for a smaller range in surface area than for the DPPC system with LL-37. This suggests that when the LL-37 is observed in the DPPC monolayer the additional phase transition is due only to the LL-37 and that there is little interaction with the DPPC and that for the case of the DPPG monolayer, the SMAP-29 physically interacts with the DPPG forming a combined DPPG/LL-37 phase transition (Fig. 5). Secondly, the pure DPPG and DPPG with SMAP-29 isotherms (Fig. 5B) do not come close to each other in values until a pressure of around 50 mN/m is reached and shortly after this the pure DPPG monolayer collapses. In addition, the isotherm of the DPPG with SMAP-29 experiment shows that the monolayer is significantly more stable as it can withstand compression to 70 mN/m. In contrast to this, the DPPC with SMAP-29 layer collapsed at a lower pressure than the pure DPPC monolayer. These data suggest stronger peptide–lipid interactions than lipid-lipid interactions in the DPPG monolayer after SMAP-29 introduction into the system. This is unlike the DPPG with LL-37 system (Fig. 5A) which underwent collapse at a much earlier stage than the DPPG alone, suggesting that although both LL-37 and SMAP-29 peptides belong to the same family of antimicrobial peptides and are α-helical, there are some differences between their modes of interaction with membranes.

On examination of the 3D structures and peptide sequence of LL-37 and SMAP-29, a structural analysis of the two peptides can be carried out to help predict how they interact with lipid monolayers. When the 3D structure of LL-37 is studied in structure-inducing environments such as lipid vesicles [49–50], it can be seen to be primarily α-helical, with a helix-bend-helix structure with the bend at residues 14–16 [49]. This makes the molecule have a curved cylindrical shape, with the hydrophobic residues residing within the

concave face of the peptide and the hydrophilic residues on the opposite surface [51]. This would allow the peptide to insert into the DPPG monolayer with the more hydrophilic side facing the subphase and the more hydrophobic side facing the tail groups of the lipid monolayer. From this 3D structure and the amino acid and charge distribution we can predict that the peptide will insert into the lipid monolayer via the carpet mechanism as we have suggested previously [7] and as has more recently been suggested when studying lipid vesicles [51]. In addition, the hydrophilic amino acids coincide with the majority of the positively charged amino acids found on the opposite side of the molecule to the hydrophobic residues and so this is where any interactions with negatively charged headgroups due to electrostatic forces would occur.

On analysis of the SMAP-29 structure it can also be seen to have a hinge, (or bend) at its centre, but the two parts of the peptide either side of the hinge have different structures where one part is α-helical and the other is an ordered hydrophobic region [9]. Although SMAP-29 has a similar percentage of hydrophobic residues as LL-37, it has 16% more hydrophilic residues, suggesting that the peptide may have greater affinity for the lipid headgroups and not penetrate into the hydrocarbon lipid tail groups to the same degree as LL-37. In addition, the SMAP-29 molecule is shorter but has a greater diameter than LL-37. This may also be a factor as to why LL-37 seems to penetrate lipid monolayers more disruptively than SMAP-29.

3.3.2. Insertion isotherms

Insertion isotherms with DPPC and DPPG systems using the LL-37 peptide have been previously published [7]. Insertion isotherms using DPPG monolayers showed that there was a substantial increase in area on peptide insertion (under constant pressure conditions at 30 mN/m) [7]. For the case of 8.9 nM LL-37 there was an increase of approximately 40% $\Delta A/A$ which rose to around 180% $\Delta A/A$ when 22.3 nM LL-37 was used.

Fig. 6 shows the insertion assay data for the DPPG with 30.7 nM SMAP-29 system at 30 mN/m under constant pressure conditions. It also shows the data for the DPPG with 8.9 and 22.3 nM LL-37 system for comparison. The increase in area of the DPPG with 30.7 nM SMAP-29 system (Fig. 6) is similar to that of 8.9 nM LL-37 into DPPG monolayer [7], which reaches approximately 40% $\Delta A/A$ after 10 min (Fig. 6). However, since SMAP-29 is more cationic than LL-37 and the fact that a higher concentration of SMAP-29 than LL-37 was used it could be expected that there would be more insertion with SMAP-29 than LL-37. However, this was not the case and there is a lower increase in area with insertion of 30.7 nM SMAP-29 in comparison to insertion of the higher concentration of LL-37 [7]. This could be attributable to a difference in peptide conformation since the number of molecules is higher in the case of SMAP-29 than in the case of LL-37 as previously mentioned. It is known that SMAP-29 has a hinge in its structure [9], allowing it to bend over on itself. However, the LL-37 molecule consists of two helical regions joined by a bend, suggesting that the LL-37 peptide remains in a more linear structure than SMAP-29 and in this way possibly facilitating insertion between DPPG molecules.

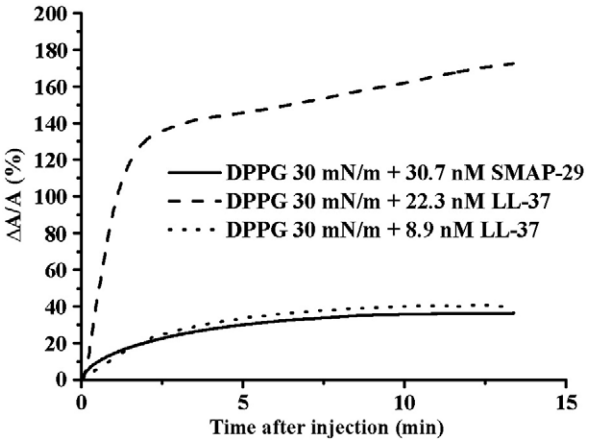

Fig. 6. Constant pressure insertion isotherm of DPPG at 30 mN/m with 30.7 nM SMAP 29.

3.3.3. Grazing incidence X-ray diffraction

Fig. 7 shows the GIXD data before (Fig. 7A) and after (Fig. 7B–C) SMAP-29 insertion into a DPPG monolayer at 30 mN/m at the lower and higher concentrations of SMAP-29, respectively. A small increase in area per molecule from 45.2 Å^2 for a pure DPPG monolayer to 46.4 Å^2 for the same system after insertion of 12.3 nM SMAP-29 was observed (Fig. 7B). This small change suggests that the DPPG structure remains largely unchanged, shown by the Bragg peaks which demonstrate the presence of an ordered structure (Fig. 7B). It should be noted that the GIXD DPPG control data presented (Fig. 7A) were previously published (Fig. 6, B1 [7]) when comparing the DPPG monolayer before and after injection of LL-37 peptide.

No Bragg peaks or rods were observed after injection of 30.7 nM SMAP-29 under the DPPG monolayer at 30 mN/m, indicating that the ordered structure of the DPPG monolayer was totally disrupted by SMAP-29 (Fig. 7C). The effect of 30.7 nM SMAP-29 on the DPPG monolayer is similar to that of the LL-37 peptide at 8.9 nM [7]. However, the higher 30.7 nM concentration of SMAP-29 was required to have the same disruptive effect as LL-37 at 8.9 nM [7]. It should be noted that the number of SMAP-29 molecules present is 38% higher than the number of LL-37 molecules at the same concentration (due to the lower molecular mass of SMAP-29). This means that if the SMAP-29 at 30.7 nM has the same effect as LL-37 (8.9 nM) on lipid monolayers, the LL-37 peptide would actually be more potent than SMAP-29 as less molecules would be required to have the same result. As was suggested from the insertion data (Fig. 6), this effective lower potency of SMAP-29 than LL-37 may be due to the structural properties of the SMAP-29 peptide, which requires a higher concentration to have a pronounced effect on the DPPG monolayer.

3.3.4. X-ray reflectivity

Fig. 8 shows the XR profiles for the DPPG system at 30 mN/m before and after injection of SMAP-29 at 30.7 nM. The data fitting for the DPPG monolayer yielded values of 18.1 Å and 5.9 Å for the tail slab and head group slab thicknesses respectively. The normalised electron density values for the tail and head group slabs were 0.98 and 1.55, respectively [7]. The XR profile after injection of SMAP-29 is very different from that of the DPPG monolayer alone (Fig. 8). This result is similar to the DPPG with 8.9 nM LL-37 case [7] and is corroborated by the GIXD results (Fig. 7C). However, the concentration of SMAP-29 (30.7 nM) used to disrupt the DPPG monolayer was higher than the concentration of LL-37 (8.9 nM) needed to disrupt the monolayer to a similar extent. The difference in concentration corresponds to nearly three and half times more SMAP-29 molecules than LL-37 molecules. The minimum of the experimental data curve was also shifted to a greater q_z value for the DPPG system with SMAP-29 in comparison to the curve for the pure DPPG monolayer. However, the shift was only 0.06 Å^{-1} in comparison to the 0.11 Å^{-1} shift of the DPPG with LL-37 system [7]. Despite this difference, the shift indicates a decrease in monolayer thickness as was seen before with the DPPG with LL-37 system [7] and as is also similar to observations by Lee et al. [52] who studied lipid systems with alamethicin and melittin peptides.

Although the shape of the second peak has dramatically changed (Fig. 8), it was still possible to fit the data using a two-slab model. The top slab has been modelled as the lipid tail groups with peptide inserted slightly into the hydrocarbon tail region and the second slab has been modelled as a mix of head groups and peptide. The fit parameters gave 16.6 Å for a thickness of the top slab (the slab closest

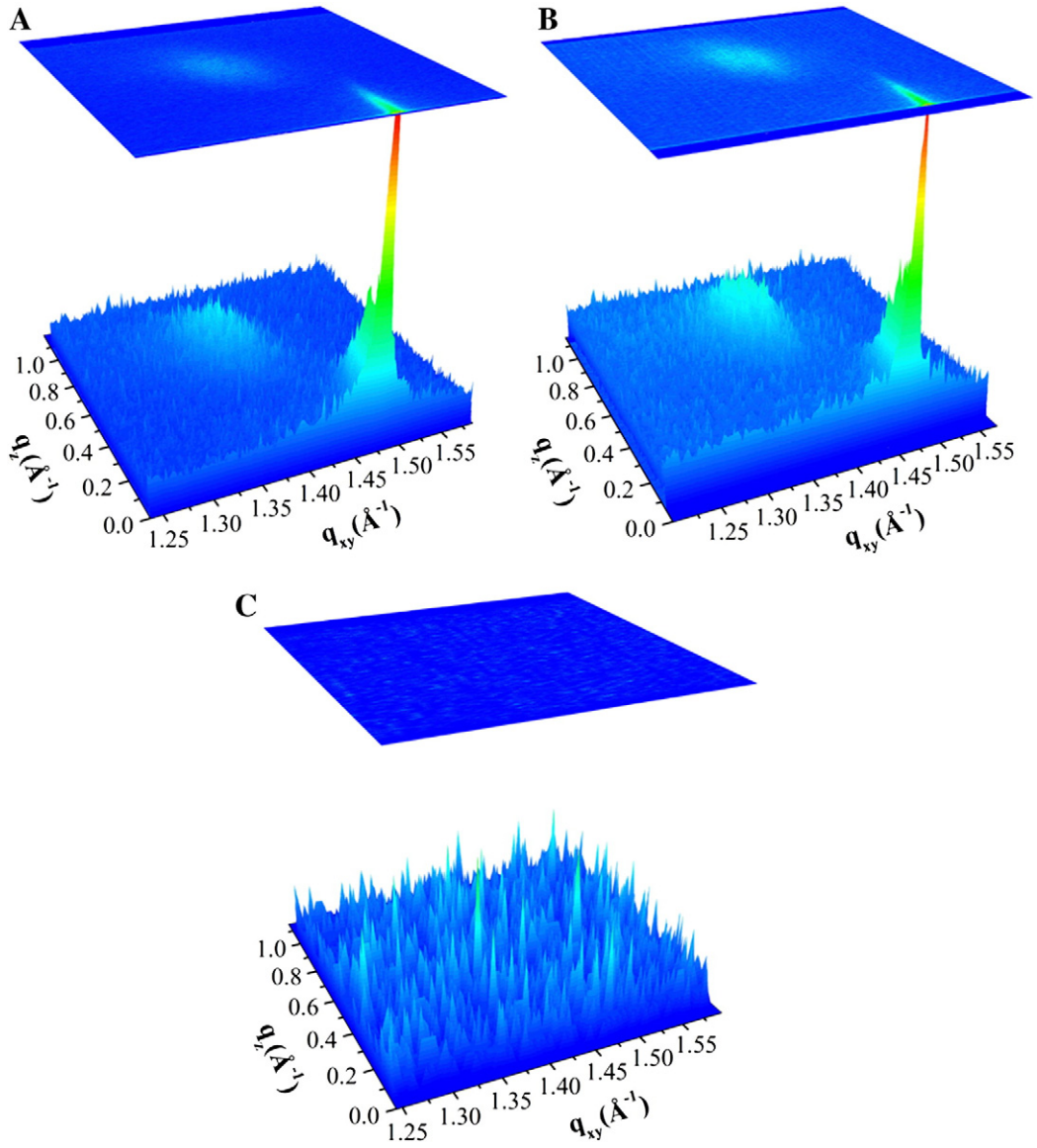

Fig. 7. 3D plots of Bragg peaks (q_{xy}) against Bragg rods (q_z) as a function of intensity. (A) DPPG 30 mN/m monolayer before injection. (B) DPPG monolayer at 30 mN/m after injection of 12.3 nM SMAP 29. (C) DPPG monolayer at 30 mN/m after injection of 30.7 nM SMAP-29.

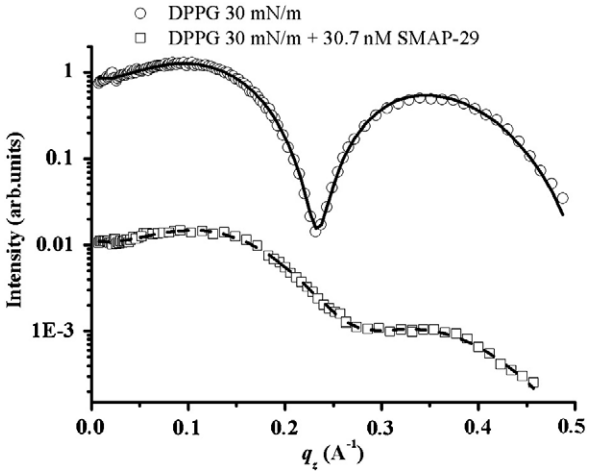

Fig. 8. X-ray specular reflectivity data (symbols) and corresponding fits (lines) normalised by Fresnel reflectivity plotted against scattering vector q_z. Data of DPPG monolayer at 30 mN/m before injection (squares) and after 30.7 Nm SMAP-29 injection (triangles). For clarity the data have been offset vertically.

to the air) with a normalised electron density of 1.17 and a second slab with a thickness of 5.9 Å and a normalised electron density of 1.25. The comparison of these values of thickness and electron density with those of the pure DPPG monolayer suggest that the peptide has fully penetrated the DPPG monolayer, as the tail group electron density has increased by almost 19%, as well as the substantial decrease (24%) in electron density in the head group slab.

In summary, the XR data show that SMAP-29 interacts strongly with DPPG lipids. This interaction results in SMAP-29 insertion into the DPPG monolayer. However, the extent of the interaction of the DPPG with SMAP-29 system is less than that of the DPPG system with LL-37, even though there are many more molecules of SMAP-29 injected into the subphase, than LL-37. These results suggest that although SMAP-29 is more cationic than LL-37, there are other factors which drive the lipid/peptide interactions such as peptide size, amino acid sequence and structure.

3.4. Schematic cartoons

Analysis of the X-ray reflectivity data showed that the SMAP-29 film consists of two slabs of similar thickness, the upper having a

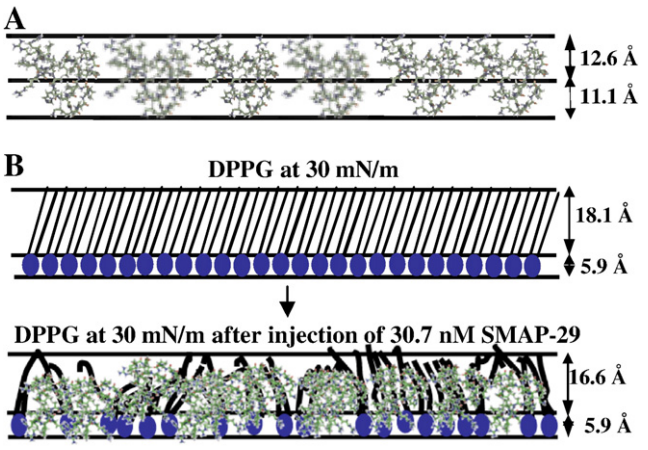

Fig. 9. (A) Cartoon schematic of possible orientation of SMAP-29 at the air aqueous interface at 1 mN/m. (B) Cartoon schematic of possible interactions of SMAP-29 with DPPG monolayer at 30 mN/m.

higher electron density than the lower. This is schematically represented in Fig. 9A, where the orientation of the SMAP-29 molecule is shown. The upper most part of the peptide contains more atoms than the lower part, thus allowing for the difference in electron density of the two slabs.

The combination of data from pretreatment experiments, insertion assays and X-ray scattering techniques can be used in order to produce a hypothesis of how SMAP-29 interacts with different lipid monolayers. It is likely that SMAP-29 interacts with the DPPC monolayer in a similar way to LL-37 [7] in that the peptide mostly remains in the subphase and there is little interaction with the DPPC monolayer.

Fig. 9B shows a schematic cartoon of the proposed mode of interaction of SMAP-29 with a DPPG monolayer at 30 mN/m based predominantly on results from X-ray scattering data. The DPPG monolayer has a tightly packed ordered structure at 30 mN/m. This is disrupted after injection of 30.7 nM SMAP-29 into the subphase, as the peptide penetrates the DPPG monolayer. The effect of SMAP-29 peptide insertion on the DPPG monolayer results in an overall thinning of the film and this thinning was also observed with a DPPG with LL-37 system at the same pressure, but to a greater extent [7]. The results suggest that it is likely that the peptide penetrates the lipid monolayer, as was the case with the LL-37 insertion into DPPG monolayers at 30 mN/m [7]. However, nearly three and a half times the number of molecules of SMAP-29 were required to have a similar effect to that of LL-37 since a concentration of 30.7 nM SMAP-29 was needed compared to 8.9 nM LL-37 and this may be due to differences in the structures of LL-37 and SMAP-29.

In conclusion, this is the first study where X-ray reflectivity and grazing incidence X-ray diffraction have been used to observe the effects of the antimicrobial peptide SMAP-29 on phospholipid monolayers at the air–aqueous interface. The experimental techniques were utilised in order to examine the principles of LL-37 and SMAP-29 cell selectivity and to investigate their mechanism of action. It was found that SMAP-29 discriminates against phospholipid monolayers containing negatively charged lipids as LL-37 does. However, when the interactions of two cathelicidin peptides with phospholipid monolayers were compared it can be seen that the LL-37 peptide has a more potent effect than the SMAP-29 peptide. This is observed from the fact that a higher concentration of SMAP-29 corresponding to nearly three and a half times as many molecules of LL-37 was required to show the same disruptive effect on DPPG monolayers. Since the SMAP-29 peptide has a higher net positive charge than LL-37, it would be expected that the SMAP-29 peptide would be more attracted to the negatively charged lipid monolayers and ensure a higher concentration near the monolayer compared to the bulk SMAP-29 concentration and the amount of LL-37 attracted to the DPPG monolayer. If a greater concentration of SMAP-29 at the lipid monolayer was present it could be proposed that SMAP-29 should interact with the monolayer to a greater extent than the LL-37 peptide. However, this was not the case and this suggests that peptide adsorption and interactions of LL-37 with lipid monolayers involve other factors such as hydrophobicity, size and charge distribution. This suggests that antimicrobial peptides interact with lipid monolayers and bilayers for a number of reasons and that is still a great deal of work to be done in the area if these peptides and their mimics are to be used as therapeutic drugs.

Acknowledgements

We thank Jeff Keen and Deidre Devine for providing the peptides. We are indebted to Chris Hodges, Yuji Ishitsuka and Ka Yee Lee for their help with ESRF measurements. We acknowledge the European Synchrotron Radiation Facility for provision of synchrotron radiation facilities at the ID10B beamline. This project was sponsored by the Engineering and Physical Sciences Research Council (GR/R86874/01), and NIH (R01 AI073892).

Appendix A. Supplementary data

Supplementary data associated with this article can be found, in the online version, at doi:10.1016/j.bbamem.2009.09.017.

References

[1] A. Giuliani, G. Pirri, A. Bozzi, A. Di Giulio, M. Aschi, A.C. Rinaldi, Antimicrobial peptides: natural templates for synthetic membrane-active compounds, Cell. Mol. Life Sci. 65 (2008) 2450–2460.
[2] D.W. Hoskin, A. Ramamoorthy, Studies on anticancer activities of antimicrobial peptides, Biochim. Biophys. Acta 1778 (2008) 357–375.
[3] N.P. Chongsiriwatana, J.A. Patch, A.M. Czyzewski, M.T. Dohm, A. Ivankin, D. Gidalevitz, R.N. Zuckermann, A.E. Barron, Peptoids that mimic the structure, function, and mechanism of helical antimicrobial peptides, Proc. Natl. Acad. Sci. U.S.A. 105 (2008) 2794–2799.
[4] K. Matsuzaki, Control of cell selectivity of antimicrobial peptides, Biochim. Biophys. Acta, Biomembr. 1788 (2009) 1687–1692.
[5] K. Lohner, E.J. Prenner, Differential scanning calorimetry and X-ray diffraction studies of the specificity of the interaction of antimicrobial peptides with membrane-mimetic systems, Biochim. Biophys. Acta 1462 (1999) 141–156.
[6] F. Neville, Y. Ishitsuka, C.S. Hodges, O. Konovalov, A.J. Waring, R. Lehrer, K.Y.C. Lee, D. Gidalevitz, Protegrin interaction with lipid monolayers: grazing incidence X-ray diffraction and X-ray reflectivity study, Soft Mater. 4 (2008) 1665–1674.
[7] F. Neville, M. Cahuzac, O. Konovalov, I. Ishitsuka, K.Y.C. Lee, G.M. Kale, D. Gidalevitz, Lipid headgroup discrimination by antimicrobial peptide LL-37: insight into mechanism of action, Biophys. J. 90 (2006) 1275–1287.
[8] B. Skerlavaj, M. Benincasa, A. Risso, M. Zanetti, R. Gennaro, SMAP-29: a potent antibacterial and antifungal peptide from sheep leukocytes, FEBS Lett. 423 (1999) 58–62.
[9] B.F. Tack, M.V. Sawai, W.R. Kearney, A.D. Robertson, M.A. Sherman, W. Wang, T. Hong, M.B. Lee, H. Wu, A.J. Waring, R.I. Lehrer, SMAP-29 has two LPS-binding sites and a central hinge, Eur. J. Biochem. 269 (2002) 1181–1189.
[10] G.H. Gudmundsson, B. Agerberth, J. Odeberg, T. Bergman, B. Olsson, R. Salcedo, The human gene FALL39 and processing of the cathelin precursor to the antibacterial peptide LL-37 in granulocytes, Eur. J. Biochem. 238 (1996) 325–332.
[11] J. Turner, Y. Cho, N.N. Dinh, A.J. Waring, R.I. Lehrer, Activities of LL 37, a cathelin-associated antimicrobial peptide of human neutrophils, Antimicrob. Agents Chemother. 42 (1998) 2206–2214.
[12] D.M.E. Bowdish, D.J. Davidson, Y.E. Lau, K. Lee, M.G. Scott, R.E.W. Hancock, Impact of LL-37 on anti-infective immunity, J. Leukoc. Biol. 77 (2005) 451–459.
[13] L. Bagella, M. Scocchi, M. Zanetti, cDNA sequences of 3 sheep myeloid cathelicidins, FEBS Lett. 376 (1995) 225–228.
[14] S.M. Travis, N.N. Anderson, W.R. Forsyth, C. Espiritu, B.D. Conway, E.P. Greenberg, P.B. McCray, R.I. Lehrer, M.J Welsh, B.F. Tack, Bactericidal activity of mammalian cathelicidin-derived peptides, Infect. Immun. 68 (2000) 2748–2755.
[15] K.A. Brogden, M. Ackermann, J. McCray, B. Paul, B.F. Tack, Antimicrobial peptides in animals and their role in host defences, Int. J. Antimicrob. Agents 22 (2003) 465–478.
[16] A. Giacometti, O. Cirioni, M.S. Del Prete, B. Skerlavaj, R. Circo, M. Zanetti, G. Scalise, *In vitro* effect on *Cryptosporidium parvum* of short-term exposure to cathelicidin peptides, J. Antimicrob. Chemother. 51 (2003) 843–847.
[17] D.G. Lee, P.I. Kim, Y. Park, S.C. Park, E.R. Woo, K.S. Hahm, Antifungal mechanism of SMAP-29 (1-18) isolated from sheep myeloid mRNA against *Trichosporon beigelii*, Biochem. Biophys. Res. Comm. 295 (2002) 591–596.

[18] B.S. McGwire, C.L. Olson, B.F. Tack, D.M. Engman, Killing of African trypanosomes by antimicrobial peptides, J. Infect. Dis. 188 (2003) 142–152.
[19] R.C. Anderson, R.E.W. Hancock, P.-L. Yu, Antimicrobial activity and bacterial-membrane interaction of ovine-derived cathelicidins, Antimicrob. Agents. Chemother. 48 (2004) 673–676.
[20] Z. Oren, J.C. Lerman, G.H. Gudmundsson, B. Agerberth, Y. Shai, Structure and organization of the human antimicrobial peptide LL-37 in phospholipid membranes: relevance to the molecular basis for its non-cell-selective activity, Biochem. J. 341 (1999) 501–513.
[21] K.A. Henzler Wildman, G.V. Martinez, M.F. Brown, A. Ramamoorthy, Perturbation of the hydrophobic core of lipid bilayers by the human antimicrobial peptide LL-37, Biochemistry 43 (2004) 8429–8459.
[22] N. Papo, Y. Shai, Host defense peptides as new weapons in the cancer treatment, Cell. Mol. Life Sci. 62 (2005) 784–790.
[23] E. Sevcsik, G. Pabst, A. Jilek, K. Lohner, How lipids influence the mode of action of membrane-active peptides, Biochim. Biophys. Acta, Biomembr. 1768 (2007) 2586–2595.
[24] E. Sevcsik, G. Pabst, W. Richter, S. Danner, H. Amenitsch, K. Lohner, Interaction of LL-37 with model membrane systems of different complexity—influence of the lipid matrix, Biophys. J. 94 (2008) 4688–4699.
[25] M. Zasloff, Antimicrobial peptides of multicellular organisms, Nature 415 (2002) 389–395.
[26] J. Seelig, Titration calorimetry of lipid–peptide interactions, Biochim. Biophys. Acta, Biomembr. 1331 (1997) 103–116.
[27] J. Seelig, Thermodyamics of lipid–peptide interactions, Biochim. Biophys. Acta, Biomembr. 1666 (2004) 40–50.
[28] O. Konovalov, I. Myagkov, B. Struth, K. Lohner, Lipid discrimination in phospholipid monolayers by the antimicrobial frog skin peptide PGLa. A synchrotron X ray grazing incidence and reflectivity study, Eur. Biophys. J. Biophys. Lett. 31 (2002) 428–437.
[29] H. Brockman, Lipid monolayers: why use half a membrane to characterize protein-membrane interactions? Curr. Opin. Struct. Biol. 9 (1999) 438–443.
[30] T.R. Jensen, K. Balashev, T. Bjornholm, K. Kjaer, Novel methods for studying lipids and lipases and their mutual interaction at interfaces. Part II. Surface sensitive synchrotron X-ray scattering, Biochimie 83 (2001) 399–408.
[31] M. Losche, Surface-sensitive X-ray and neutron scattering characterization of planar lipid model membranes and lipid/peptide interactions, Curr. Top. Membr. 52 (2002) 117–161.
[32] F. Sun, Constant normal pressure, constant surface tension, and constant temperature molecular dynamics simulation of hydrated 1, 2-dilignoceroyl-phosphatidylcholine monolayer, Biophys. J. 82 (2002) 2511–2519.
[33] E.E. Ambroggio, F. Separovic, J. Bowie, G.D. Fidelio, Surface behaviour and peptide–lipid interactions of the antibiotic peptides, maculatin and citropin, Biochim. Biophys. Acta 1664 (2004) 31–37.
[34] F. Neville, C.S. Hodges, C. Liu, O. Konovalov, G.M. Kale, D. Gidalevitz, In situ characterization of lipid A interaction with antimicrobial peptides using surface X-ray scattering, Biochim. Biophys. Acta 1758 (2006) 232–240.
[35] S.A. Maskarinec, J. Hannig, R.C. Lee, K.Y.C. Lee, Direct observation of poloxamer 188 insertion into lipid monolayers. Biophys. J. 82 (2002) 1453–1459.
[36] G. Wu, J. Majewski, C. Ege, K. Kjaer, M.J. Weygand, K.Y.C. Lee, Lipid corralling and poloxamer squeeze-out in membranes, Phys. Rev. Lett. 93 (2004) 028101.
[37] R.A. Demel, W.S.M. Geurts van Kessel, R.F.A. Zwaal, B. Roelofsen, L.LM. van Deenen, Relation between various phospholipase actions on human red cell membranes and the interfacial phospholipid pressure in monolayers, Biochim. Biophys. Acta 406 (1975) 97–107.
[38] A. Blume, A comparative study of the phase transitions of phospholipid bilayers and monolayers, Biochim. Biophys. Acta 557 (1979) 32–44.
[39] R. Gennaro, M. Zanetti, Structural features and biological activities of the cathelicidin-derived antimicrobial peptides, Biopolymers 55 (2000) 31–49.
[40] A. Gopal, K.Y.C. Lee, Morphology and collapse transitions in binary phospholipid monolayers, J. Phys. Chem., B 105 (2001) 10348–10354.
[41] D. Gidalevitz, Y.J. Ishitsuka, A.S. Muresan, O. Konovalov, A.J. Waring, R.I. Lehrer, K. Y.C. Lee, Interaction of antimicrobial peptide protegrin with biomembranes, Proc. Natl. Acad. Sci. U.S.A. 100 (2003) 6302–6307.
[42] O. Konovalov, S.M. O'Flaherty, E. Saint-Martin, G. Deutsch, E. Sevcsik, K. Lohner, The bending rigidity of phospholipid monolayers in presence of an antimicrobial frog peptide studied by X-ray grazing incidence diffraction, Physica B 357 (2005) 185–189.
[43] J. Als-Nielsen, D. McMorrow, Elements of modern X-ray physics, John Wiley & Sons, Chichester, 2001.
[44] T.R. Jensen, K. Kjaer, Structural properties and interactions of thin films at the air–liquid interface explored by synchrotron X-ray scattering, in: D. Möbius, R. Miller (Eds.), Novel Methods to Study Interfacial Layers, 11, Elsevier B.V., Amsterdam, 2001.
[45] M. Schalke, M. Losche, Structural models of lipid surface monolayers from X-ray and neutron reflectivity measurements, Adv. Colloid Interface Sci. 88 (2000) 243–274.
[46] C.A. Helm, H. Möhwald, K. Kjaer, J. Als-Nielsen, Phospholipid monolayer density distribution perpendicular to the water surface. A Synchrotron X-Ray Reflectivity Study, Europhys. Lett. 4 (1987) 697–703.
[47] J. Als-Nielsen, D. Jacquemain, K. Kjaer, F. Leveiller, M. Lahav, L. Leiserowitz, Principles and applications of grazing incidence X-ray and neutron scattering from ordered molecular monolayers at the air–water interface, Phys. Rep. 242 (1994) 251–313.
[48] D. Gidalevitz, Z.Q. Huang, S.A. Rice, Protein folding at the air–water interface studied with X-ray reflectivity, Proc. Natl. Acad. Sci. U.S.A. 96 (1999) 2608–2611.
[49] S.L. Keller, W.H. Pitcher, W.H. Huestis, H.M. McConnell, Red blood cell lipids form immiscible liquids, Phys. Rev. Lett. 81 (1998) 5019–5022.
[50] G. Wang, Structures of human host defense cathelicidin LL-37 and its smallest antimicrobial peptide KR-12 in lipid micelles, J. Biol. Chem. 283 (2008) 32637–32643.
[51] F. Porcelli, R. Verardi, L. Shi, K.A. Henzler-Wildman, A. Ramamoorthy, G. Veglia, NMR structure of the cathelicidin-derived human antimicrobial peptide LL-37 in dodecylphosphocholine micelles, Biochemistry 47 (2008) 5565–5572.
[52] M.T. Lee, F.Y. Chen, H.W. Huang, Energetics of pore formation induced by membrane active peptides, Biochemistry 43 (2004) 3590–3599.